Inorg. Chem. **2005**, *44*, 8343–8348

Scanning Probe Microscopy Characterization of Single Chains Based on a One-Dimensional Oxalato-Bridged Manganese(II) Complex with 4-Aminotriazole

Urko García-Couceiro,[†] David Olea,[‡] Oscar Castillo,*[,†] Antonio Luque,[†] Pascual Román,[†] Pedro J. de Pablo,[‡] Julio Gómez-Herrero,[‡] and Félix Zamora*[,§]

Departamento de Química Inorgánica, Universidad del País Vasco, Apartado 644, E-48080 Bilbao, Spain, Departamento de Física de la Materia Condensada, Universidad Autónoma de Madrid, E-28049 Madrid, Spain, and Departamento de Química Inorgánica (C-VIII), Universidad Autónoma de Madrid, E-28049 Madrid, Spain

Received April 7, 2005

The compound $[Mn(\mu\text{-ox})(4atr)_2]_n$ (**1**) (ox = oxalato and 4atr = 4-amine-1,2,4-triazole) has been synthesized and characterized by FT-IR spectroscopy, thermal analysis, variable-temperature magnetic measurements, and X-ray single-crystal diffraction methods. The crystal structure of compound **1** consists of one-dimensional linear chains in which *trans*-$[Mn(4atr)_2]^{2+}$ units are sequentially bridged by centrosymmetric bis-bidentate oxalato ligands. Cryomagnetic measurements show an overall antiferromagnetic behavior of the compound. Isolated chains of this polymer have been obtained by sonication of **1** in ethanol or treatment of the polymer with NaOH and morphologically characterized on highly oriented pyrolitic graphite and mica surfaces by atomic force microscopy and scanning tunneling microscopy. The procedures employed to obtain single chains of this coordination polymer open a route for future nanotechnological applications of these types of materials.

Introduction

The design and synthesis of one-dimensional (1D) coordination polymers have been particularly active because of the prospects of generating new materials with interesting structural properties in areas such as electronics, photochemistry, and magnetochemistry.[1] However, the application of coordination polymers is mainly limited by their restricted processability, as a consequence of their lack of solubility, rapid degradation in solution, and decomposition upon heating.[1] Few methods have been reported for the isolation of these metal−organic chains, although 1D nanostructures (such as wires, rods, and tubes) have attracted extensive interest in recent years.[2] However, the studies of the properties on coordination polymers have been carried out to a macroscopic scale. For instance, studies on electrical conduction are very scarce and are limited to monocrystals or pellets of these polymers.[3] 1D coordination polymers are of special interest for nanotechnology because individual chains of these polymers could be used as molecular wires with a number of advantages over other materials such as carbon nanotubes, due to their easier synthesis, or higher reactivity. It is possible to modify the bulk magnetic, electronic, and optical properties of these 1D polymers by tailoring the molecules.[4−7] However, research on coordination polymers on solid surfaces is in its infancy. The isolation of single chains of 1D coordination polymers seems to be more restricted than that of 2D arrays.

* To whom correspondence should be addressed. E-mail: oscar.castillo@ehu.es (O.C.), felix.zamora@uam.es (F.Z.).

[†] Universidad del País Vasco.

[‡] Departamento de Física de la Materia Condensada, Universidad Autónoma de Madrid.

[§] Departamento de Química Inorgánica (C-VIII), Universidad Autónoma de Madrid.

(1) Janiak, C. *J. Chem. Soc., Dalton Trans.* **2003**, 2781.

(2) Xia, Y.; Yang, P.; Sun, Y.; Wu, Y.; Mayers, B.; Gates, B.; Yin, Y.; Kim, F.; Yan, H. *Adv. Mater*. **2003**, *15*, 353.

(3) Kitagawa, H.; Onodera, N.; Sonoyama, T.; Yamamoto, M.; Fukawa, T.; Mitani, T.; Seto, M.; Maeda, K. *J. Am. Chem. Soc.* **1999**, *121*, 10068.

(4) Kahn, O. *Molecular Magnetism*; VCH: New York, 1993.

(5) Miller, J. S., Ed. *Extended Linear Chain Compounds*; Plenum: New York, 1982; Vol. 3.

(6) Delhaes, P., Drillon, M., Eds. *Organic and Inorganic Linear Dimensional Crystalline Materials*; NATO Advanced Study Institute Series 168; NATO: New York, 1989.

(7) Shen, H. Y.; Bu, W. M.; Gao, E. Q.; Liao, D. Z.; Jiang, Z. H.; Yan, S. P.; Wang, G. L. *Inorg. Chem.* **2000**, *39*, 396.

10.1021/ic0505302 CCC: $30.25
Published on Web 10/14/2005

Experimental Section

Materials. All chemicals were of reagent grade and were used as commercially obtained. Elemental analyses (C, H, N) were performed on a LECO CHNS-932 microanalytical analyzer. The metal content was determined by absorption spectrometry.

Synthesis of [Mn(μ-ox)(4atr)$_2$]$_n$ (1). Pale-pink single crystals of **1** were obtained by the slow evaporation of an aqueous solution containing $Mn(NO_3)_2 \cdot 4H_2O$ (0.050 g, 0.20 mmol), 4atr (0.084 g, 1.00 mmol), and $K_3[Cr(ox)_3] \cdot 3H_2O$ (0.098 g, 0.20 mmol) as the oxalato source. Yield: 20% (based on Mn). Anal. Calcd for $C_6H_8MnN_8O_4$: C, 23.16; H, 2.59; N, 36.02; Mn, 17.66. Found: C, 22.95; H, 2.48; N, 35.89; Mn, 17.51. Main IR features (cm^{-1}, KBr pellet): 3335s and 3225s for ν(N−H); 3115s for ν(C−H); 1620vs for $\nu_{as}(CO_2)$; 1525m and 1460w for ν_{as}(C═N); 1365m and 1320s for $\nu_s(CO_2)$; 1210m, 1195m, and 1075m for δ_{ip}(C−H); 995m for ν_s(CO); 955m for δ_{ring}; 895m and 850m for δ_{op}(C−H); 800s for $\delta(CO_2)$; 680m and 620s for τ_{ring}; 495m and 415m for ν(M−O + M−N).

Sample Preparation for Atomic Force Microscopy (AFM). Procedure a. [Mn(μ-ox)(4atr)$_2$]$_n$ (1 mg) was suspended in absolute ethanol (1 mL) and sonicated (680 W, 40 kHz) for 30 min at 20 °C. The suspension was centrifuged at 40 000 rpm for 10 min, and 50 μL of the clear solution was deposited on a freshly cleaved mica sheet. Then, the sample was left in air, allowing the complete evaporation of the solvent. **Procedure b.** A total of 1 mg of [Mn(μ-ox)(4atr)$_2$]$_n$ was treated with 1 mL of NaOH (0.1 mol L^{-1}). The suspension was centrifuged, and 50 μL of the clear solution was deposited on a cleaved mica sheet previously treated with (aminopropyl)triethoxysilane, left in air for 10 min and washed with water. AFM images were acquired in dynamic mode using a Nanotec Electronica system (www.nanotec.es). Olympus cantilevers were used with a nominal force constant of 0.75 N m^{-1}.

Sample Preparation for Scanning Tunneling Microscopy (STM). The sample was prepared following procedure **a**, described above, and 50 μL of the clear solution was deposited on a freshly cleaved highly oriented pyrolitic graphite (HOPG) sheet. Then, the sample was left in air, allowing the complete evaporation of ethanol. STM images were acquired at atmospheric conditions using a Nanotec Electronica system (www.nanotec.es). Mechanically cut platinum−iridium tips were used for all of the experiments.

Physical Measurements. The IR spectra (KBr pellets) were recorded on a FT-IR Mattson 1000 spectrometer in the 4000−400-cm^{-1} spectral region. Thermal analyses (TG/DTG/DTA) were performed on a TA Instruments STD 2960 thermal analyzer in a synthetic air atmosphere (79% N_2/21% O_2) with a heating rate of 5 °C min^{-1}. Magnetic measurements were performed on polycrystalline samples of the compounds with a Quantum Design SQUID susceptometer covering the temperature range of 5−300 K. The susceptibility data were corrected for the diamagnetism estimated from Pascal's tables,[8] the temperature-independent paramagnetism, and the magnetization of the sample holder.

X-ray Data Collection and Structure Determination. Data collection was carried out at 293(2) K with an Xcalibur diffractometer equipped with an area detector and using graphite monochromated Mo Kα radiation (λ = 0.710 73 Å). Data were corrected for absorption, Lorentz, and polarization effects. The structure was solved by direct methods using the SIR 97 program.[9] Full matrix least-squares refinements were performed on F^2 using SHELXL97.[10] All non-hydrogen atoms were refined anisotropically. All calculations were performed using the WINGX crystallographic software package.[11] Crystallographic data and details of the refinement are given in Table 1. Selected bond lengths and angles are listed in Table 2.

Table 1. Single-Crystal Data and Structure Refinement Details[a]

empirical formula	$C_6H_8MnN_8O_4$
formula weight	311.12
crystal system	orthorhombic
space group	*Pnmn*
a (Å)	5.599(1)
b (Å)	7.401(2)
c (Å)	14.232(4)
V (Å^3)	589.8(3)
Z	2
D_{calc} (g cm^{-3})	1.752
μ (mm^{-1})	1.147
F(000)	314
max θ (deg)	30.05
reflns collected	4971
range *h*; *k*; *l*	−7, 5; −10, 10; −20, 20
independent reflns (R_{int})	924 (0.0404)
data, restraints, param	924, 0, 65
reflns with $I \geq 2\sigma(I)$	518
goodness-of-fit *S* on F^2 [a]	0.985
final *R* indices [$I \geq 2\sigma(I)$]: R1[a]/ wR2[b]	0.0400/0.0744
R indices [all data]: R1[a]/ wR2[b]	0.1116/0.0928
largest difference peak (e Å^{-3})	0.466
largest difference hole (e Å^{-3})	−0.213

[a] $R1 = \sum(|F_o| - |F_c|)/\sum|F_o|$; $S = [\sum w(F_o^2 - F_c^2)^2/(n-p)]^{1/2}$, where *n* is the number of observed reflections and *p* is the number of parameters refined. [b] $wR2 = [\sum w(F_o^2 - F_c^2)^2/\sum w(F_o^2)^2]^{1/2}$; $w = 1/[\sigma^2(F_o^2) + (0.0372P)^2]$ with $P = (|F_o|^2 + 2|F_c|^2)/3$.

Table 2. Selected Bond Lengths (Å) and Angles (deg)[a]

Mn1−O1 × 4	2.169(2)	Mn1−N11 × 2	2.228(3)
O1−Mn1−O1^{i}	76.83(9)	O1^{ii}-Mn1−O1^{iii}	76.83(9)
O1−Mn1−O1^{ii}	180(−)	O1−Mn1−N11	89.09(6)
O1−Mn1−O1^{iii}	103.17(9)	O1−Mn1−N11^{iii}	90.91(6)
O1^{i}-Mn1−O1^{ii}	103.17(9)	N11−Mn1−N11^{iii}	180(−)
O1^{i}-Mn1−O1^{iii}	180(−)		

[a] Symmetry: i = x, $-y$, z; ii = $-x+1$, $-y$, $-z+1$; iii = $-x+1$, y, $-z+1$.

Results and Discussion

The crystal structure analysis revealed the presence of neutral linear 1D chains in which *trans*-[Mn(4atr)$_2$]$^{2+}$ units are bridged by centrosymmetric bis-bidentate oxalato ligands with a metal−metal distance of 5.599(1) Å. Mn(II) atoms, located on 2/*m* symmetry sites, are coordinated to four oxygen atoms [Mn−O1, 2.169(2) Å] from two symmetry-related oxalato ligands and two endocyclic nitrogen atoms [Mn−N11, 2.228(3) Å] of 4atr terminal ligands, giving a distorted octahedral MnO_4N_2 chromophore (Figure 1).

The 1D chains run along the *a* axis and the terminal 4atr ligands are parallel to the propagation direction of the chain because of an intramolecular weak hydrogen bond between the endocyclic N12 nitrogen atom and the C15−H group of neighboring 4atr ligands [C···N, 3.449(6) Å; C−H···N, 163(3)°]. Each chain within the unit cell of **1** is interconnected

(8) Earnshaw, A. *Introduction to Magnetochemistry*; Academic Press: London, 1968.
(9) Altomare, A.; Burla, M. C.; Camalli, M.; Cascarano, G. L.; Giacovazzo, C.; Guagliardi, A.; Moliterni, A. G. G.; Spagna, R. *J. Appl. Crystallogr.* **1999**, *32*, 115.
(10) Sheldrick, G. M. *SHELXS97 and SHELXL97*; University of Göttingen: Göttingen, Germany, 1997.
(11) Farrugia, L. J. *WINGX. A Windows program for crystal structure analysis*; University of Glasgow: Glasgow, Great Britain, 1998.

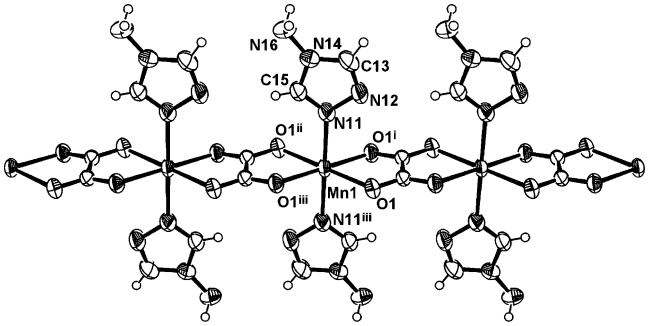

Figure 1. Diagram of the polymeric chain of compound **1**.

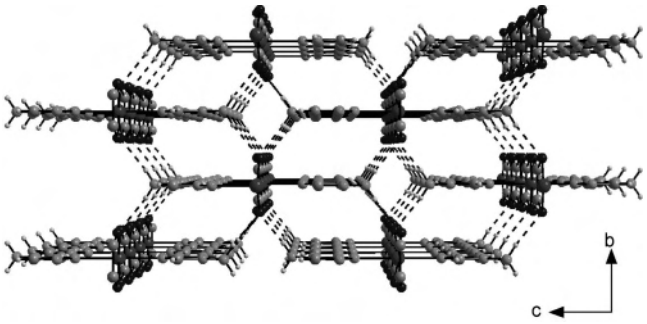

Figure 2. Packing diagram of compound **1** viewed along the crystallographic *a* axis. Hydrogen-bond contacts are represented by dashed lines.

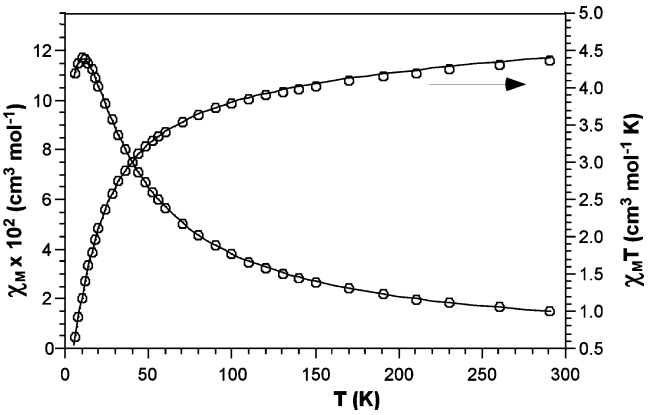

Figure 3. Plots of the thermal dependence of χ_M and $\chi_M T$ for compound **1** and the best theoretical fit (—).

to the nearest four units (Figure 2) by means of N−H···O_{ox} hydrogen bonds involving the oxalato oxygen atoms and the *exo*-amino groups of the terminal 4atr ligands [N16···O1, 2.970(3) Å]. The robustness of the supramolecular architecture is confirmed by its high thermal stability. Under an air atmosphere, compound **1** remains stable until 280 °C, and then it undergoes a very exothermic process, leading to MnO above 350 °C (see the Supporting Information).

Plots showing the thermal evolution of the magnetic molar susceptibility and the product $\chi_M T$ are presented in Figure 3 (T range, 5−300 K; applied field, 1000 G). The room-temperature value for $\chi_M T$ (4.38 $cm^3\ mol^{-1}$ K) corresponds to the spin-only value (considering $g = 2.00$) expected for a high-spin d^5 Mn(II) ion, it remains almost constant up to 100 K, and then it decreases rapidly upon further cooling. The χ_M curve increases when the compound is cooled until a maximum is reached at 11 K, and then it decreases very quickly. This dependence is indicative of antiferromagnetic

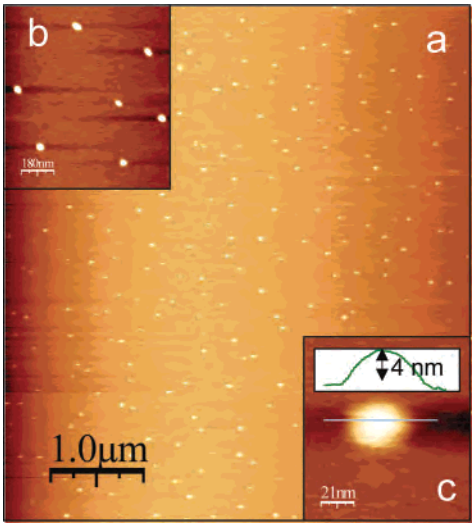

Figure 4. AFM topography image (a) with a zoomed area (b), showing the homogeneously distributed nanoparticles on mica. The height of a nanoparticle is about 4 nm (c), and the lateral dimensions are beyond the resolution of the AFM.

coupling between the Mn(II) centers through the bridging oxalato ligands. Taking into account the 1D structure of **1**, the experimental data have been fitted by means of an $S = {}^5/_2$ Fisher antiferromagnetic chain model ($H = -J\sum S_i S_{i+1}$).[12] The best-fit parameters are $J = -1.74$ cm^{-1}, $g = 2.00$, and $R = 1.3 \times 10^{-5}$ (solid line in Figure 3), where R is the agreement factor defined as $R = \sum_i[(\chi_M)_{obs}(i) - (\chi_M)_{calc}(i)]^2/\sum_i[(\chi_M)_{obs}(i)]^2$.

The magnitude of the antiferromagnetic interaction is larger than that found for the 1D $[Mn(\mu\text{-ox})(bpy)]_n$ compound ($J = -1.20$ cm^{-1}; bpy = 2,2′-bipyridine)[13] with a *cis*-MnO_4N_2 chromophore and the 1D $[Mn(\mu\text{-ox})(H_2O)_2]_n$ compound ($J = -0.88$ cm^{-1})[14] with a MnO_6 environment, but it is weaker than that ($J = -2.48$ cm^{-1}) reported[15] for the dimeric $[Mn_2(\mu\text{-ox})(bispictn)_2](ClO_4)_2$ compound [bispictn = *N*,*N*′-bis(2-pyridylmethyl)-1,3-propanediamine] with a MnO_2N_4 donor set (see the Supporting Information). A similar trend has been reported for oxalato-bridged Ni(II) complexes in which the magnitude of the exchange coupling is strongly dependent on the nature of the donor atoms in the peripheral ligands: the less electronegative they are, the greater is the antiferromagnetic coupling.[16]

1D coordination polymers are usually insoluble in most of the solvents, or their solubilization leads frequently to decomposition.[1] We have recently proved that the use of ultrasound with these types of compounds may allow the separation of the single chains.[17] In that case, the interactions between the chains were removed by means of ultrasound

(12) Fisher, M. E. *Am. J. Phys.* **1964**, *32*, 343.
(13) Deguenon, D.; Bernardinelli, G.; Tuchagues, J. P.; Castan, P. *Inorg. Chem.* **1990**, *29*, 3031.
(14) Simizu, S.; Friedberg, S. A. *J. Appl. Phys.* **1988**, *63*, 3557.
(15) Glerup, J.; Goodson, P. A.; Hodgson, D. J.; Michelsen, K. *Inorg. Chem.* **1995**, *34*, 6255.
(16) (a) Román, P.; Guzmán-Miralles, C.; Luque, A.; Beitia, J. I.; Cano, J.; Lloret, F.; Julve, M.; Alvarez, S. *Inorg. Chem.* **1996**, *35*, 3741. (b) Castillo, O.; Luque, A.; Román, P.; Lloret, F.; Julve, M. *Inorg. Chem.* **2001**, *40*, 5526. (c) Vitoria, P.; Muga, I.; Gutiérrez-Zorrilla, J. M.; Luque, A.; Román, P.; Lezama, L.; Zúñiga, J.; Beitia, J. I. *Inorg. Chem.* **2003**, *42*, 960.

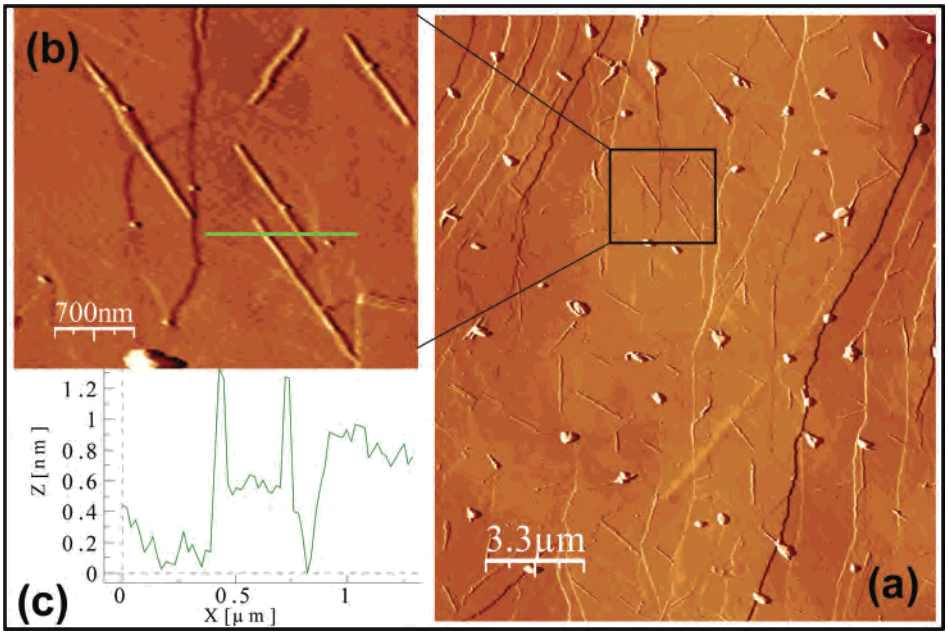

Figure 5. (a) AFM topography image of $[Mn(\mu\text{-ox})(4atr)_2]_n$ deposited on HOPG, showing a large number of chains. A high-pass filter was used to enhance the borders. (b) Zoomed area of the previous image, displaying five chains with nonuniform width. (c) Profile taken along the line in part b but in the unfiltered image. The height of the molecules is 0.8 nm above a plateau with a height of about 0.6 nm, which coincides within the *Z* piezoelectric error with a double graphite step.

techniques and single chains were isolated on a mica surface. The image taken in noncontact dynamic mode[18] showed a 0.5-nm-diameter nanofiber with a length above 1 μm.

Sonicated suspensions of compound **1** in ethanol lead to the formation of a homogeneous distribution of nanoparticles of 4 nm in height on a mica surface (Figure 4).[19] The AFM images reveal a high particle density, suggesting a high yield process. To favor the formation of linear chains, a wide range of solvents (CH_2Cl_2, $CHCl_3$, toluene, OEt_2, THF, etc.) were tested to find a different physicochemical behavior of the polymer without any significant result. In addition, we tried adsorption on a hydrophobic surface. Thus, by sonication of **1** in ethanol and deposition on HOPG, a high density of linear chains were observed by AFM (Figure 5), with height values between 0.5 and 1 nm, which is in agreement with the expected diameter of a single polymer. The *Z* piezoelectric was calibrated using the step height of graphite. However, the nonlinearities of the piezoelectrics can introduce variations in the measured heights up to 20%. Careful measurements of the angles between chains indicate that they are formed following the steps on the graphite surface because the angles are always close to 120° or 60°.[20] The AFM images in Figure 5 show that the molecule width is not uniform, suggesting that we may have more than one molecule. To check this issue, STM has been used. However,

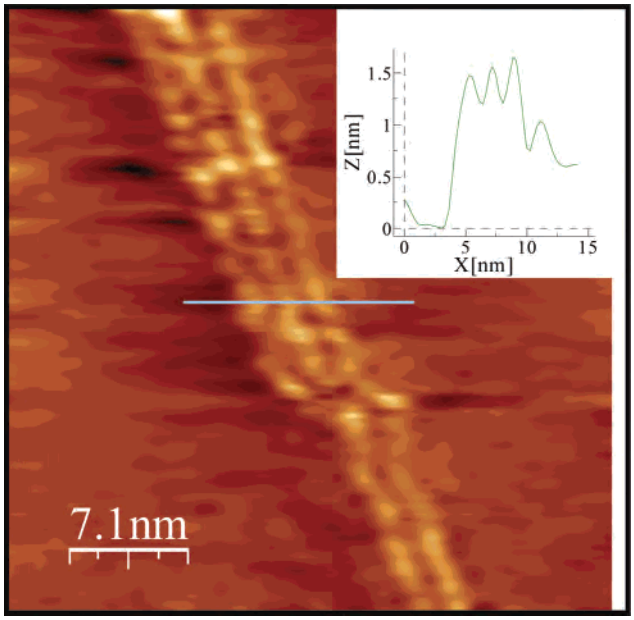

Figure 6. High-resolution STM topography showing the detail of the chains observed in Figure 5. Tunnel conditions are $I_t = 6$ nA and $V_t = 27$ mV.

we have carefully considered this possibility because we are aware of the many artifacts of STM imaging on HOPG surfaces.[21]

Figure 6 is a high-resolution STM image showing parallel structures of the coordination polymer. We have carefully considered the possibility of having a multiple tip. However, as can be seen in Figure 6, the structure evolves from three parallel linear chain structures (upper region of the image) to two parallel chains. We have also checked other chains with the same tip, finding different numbers of parallel

(17) Olea, D.; Amo-Ochoa, P.; Guijarro, A.; de Jesús, F.; Soler, J.; de Pablo, P. J.; Zamora, F.; Gómez-Herrero, J. *Adv. Mater.* **2005**, *17*, 1761.
(18) www.nanotec.es.
(19) The lateral dimensions are below the AFM resolution, which is given by the final diameter of the cantilever tip, usually about 20−30 nm. Therefore, the lateral size of these particles must be smaller than the diameter of the tip; in fact, assuming a spherical particle, its size would be the measured height, that is, 4 nm.
(20) Novokmet, S.; Alam, M. S.; Dremov, V.; Heinemann, F. W.; Muller, P.; Alsfasser, R. *Angew. Chem., Int. Ed.* **2005**, *44*, 803.
(21) Clemmer, C. R.; Beebe, T. P., Jr. *Science* **1991**, *251*, 640.

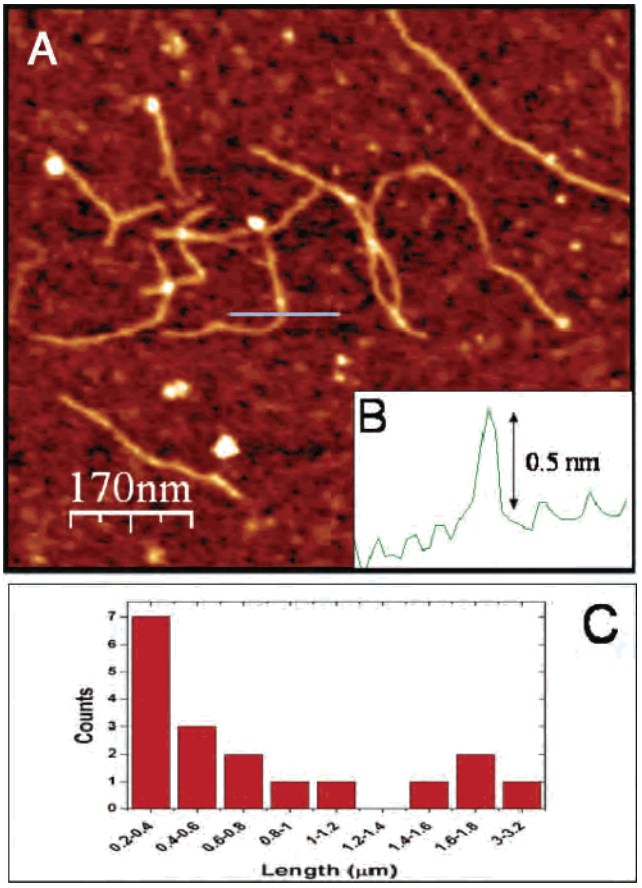

Figure 7. 850 nm × 840 nm AFM topography image (A) and height profile across the line (B) of several single chains of the $[Mn(\mu\text{-ox})(4atr)_2]_n$ polymer adsorbed on mica. (C) Number of molecules vs molecule lengths for $[Mn(\mu\text{-ox})(4atr)_2]_n$.

molecules. Therefore, we have ruled out the possibility of a multiple tip. This confirms our hypothesis of a multiple-molecule structure for each of the chains observed in the AFM images.

As another possible way to extract single chains of the polymer in water, we tried to deprotonate the 4atr-coordinated ligands with a diluted solution of NaOH (0.1 mol L^{-1}). Although a partial decomposition of the polymer takes place with the formation of Mn_3O_4, the resulting solution deposited over mica leads to single chains of compound **1** (Figure 7), with the height ranging from 0.4 to 0.6 nm (Figure 7b). This is in good agreement with the expected diameter of the chains, based on X-ray data (Figure S5 in the Supporting Information). A low density of chains is observed in the AFM images, which is an indication of a low yield process. The big particle observed at either end of the molecule can be attributed to NaOH aggregation. This also can explain the varying width of the molecule along its length. Figure 7c portrays a statistic of the molecule length. We have found that as the length of the molecules increases, the probability of finding a molecule drops. This indicates that NaOH is probably "cutting" the molecules [by oxidation of Mn(II)] as proposed above. To make sure that the linear structures are not related with some kind of product decomposition, we treated blank dispersions of 4atr and $MnCl_2$ under the same conditions (concentration, surface,

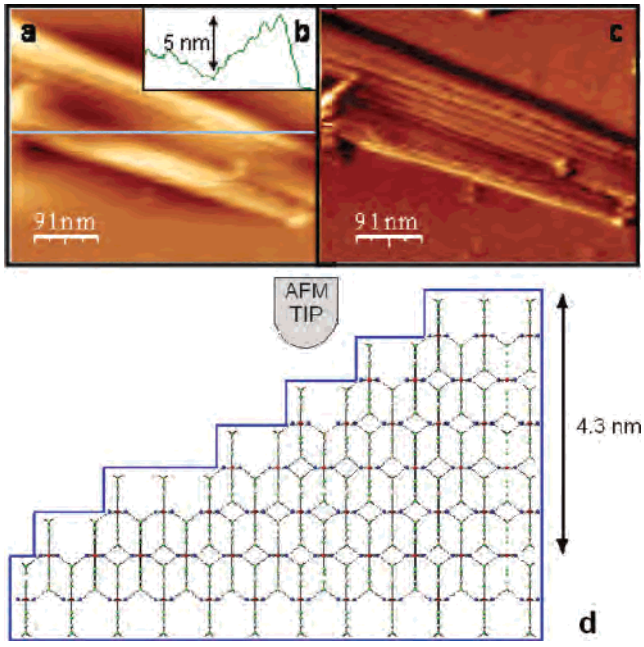

Figure 8. AFM topography image (a) and profile across the line (b) of a $[Mn(\mu\text{-ox})(4atr)_2]_n$ fragment of crystal resulting from the sonication of the original crystals. In part c, an edge-enhancement filter has been used, remarking that the crystal is built of several parallel chains. (d) Plausible explanation for the crystal morphology.

etc.) without finding any linear structure. This again suggests that we are dealing with linear polymers.

In these samples, small crystals with a fibrous nature can also be observed (Figure 8). The measured heights of the longitudinal fibers are again in good agreement with the diameter of the single chains (Figure 8d). Solutions of NaOH (0.1 mol L^{-1}), $MnCl_2$, and 4atr ligand were prepared under the same conditions and observed with AFM. Neither similar crystals nor single chains were observed. The deprotonation of the polymer with NaOH causes the liberation of the single chains and partial oxidation of Mn(II). However, the deposition and drying out of the solution stops the oxidation and allows the observation of some single molecules by AFM.

Different structures have been found during these experiments. On mica, the chains tends to minimize its exposition to this surface by forming rounded structures. On HOPG, the situation is reversed; it presents a linear structure, which is favored by the existence of steps. For both cases, the treatment of **1** implied just sonication in ethanol. However, linear chains were also obtained by deprotonation of the coordination polymer with NaOH (without sonication) and deposition on mica. The polyanion generated from **1** should have a net charge along the chains, which could produce the linear structure observed in the AFM images (Figure 7).[22] These facts seem to indicate that the nature of the substrate and the polymer plays an important role in the arrangement of the chains on the surface.

Conclusion

We report herein the synthesis, chemical characterization, and crystal structure of the 1D antiferromagnetic [Mn(μ-

(22) Gallyamov, M. O.; Tartsch, B.; Khokhlov, A. R.; Sheiko, S. S.; Borner, H. G.; Matyjaszewski, K.; Moller, M. *J. Microsc.* **2004**, *215*, 245.

ox)(4atr)$_2$]$_n$ coordination polymer. Its processability, as nanospheres and single chains, has been achieved by ultrasound or deprotonation of the coordinated 4atr ligands. This permits the morphological characterization of that polymer by AFM and STM. The results obtained open a new route for future nanotechnological applications of these types of materials.

Acknowledgment. This work was supported by the Spanish Ministerio de Ciencia y Tecnología (Grants MAT2005-03047 and MAT2004-05589-C02-01/02), NISAN/IST-2001-38052, and the Universidad del País Vasco/Euskal Herriko Unibertsitatea (9/UPV 00169.310-15329/2003). U.G-C. thanks the latter institution for a predoctoral fellowship. D.O. is grateful for financial support from NISAN/IST-2001-38052. We thank Pablo Ares and the Nanotec SL team for technical help.

Supporting Information Available: X-ray crystallographic file in CIF format, FT-IR spectrum data, TGA/DTA curves, magnetic data, and ORTEP views. This material is available free of charge via the Internet at http://pubs.acs.org.

IC0505302